

## Automatic navigation of an untethered device in the artery of a living animal using a conventional clinical magnetic resonance imaging system

Sylvain Martel,<sup>a)</sup> Jean-Baptiste Mathieu, Ouajdi Felfoul, Arnaud Chanu, Eric Aboussouan, Samer Tamaz, and Pierre Pouponneau

*NanoRobotics Laboratory, Department of Computer Engineering and Institute of Biomedical Engineering, École Polytechnique de Montréal (EPM), Campus of the Université de Montréal, P.O. Box 6079, Station Centre-Ville, Montréal, Québec H3C 3A7, Canada*

L'Hocine Yahia

*Laboratoire d'Innovation et d'Analyse de la Bioperformance (LIAB), École Polytechnique de Montréal (EPM), Campus de l'Université de Montréal, P.O. Box 6079, Station Centre-Ville, Montréal, Québec H3C 3A7, Canada*

Gilles Beaudoin and Gilles Soulez

*Department of Radiology, Centre Hospitalier de l'Université de Montréal (CHUM)—Hôpital Notre-Dame, Pavillon Lachapelle, Office C-1077, 1560 Sherbrooke Est Montréal, Québec H2L 4M1, Canada*

Martin Mankiewicz

*NanoRobotics Laboratory, Department of Computer Engineering and Institute of Biomedical Engineering, École Polytechnique de Montréal (EPM), Campus of the Université de Montréal, P.O. Box 6079, Station Centre-Ville, Montréal, Québec H3C 3A7, Canada*

(Received 1 February 2007; accepted 8 February 2007; published online 14 March 2007)

The feasibility for *in vivo* navigation of untethered devices or robots is demonstrated with the control and tracking of a 1.5 mm diameter ferromagnetic bead in the carotid artery of a living swine using a clinical magnetic resonance imaging (MRI) platform. Navigation is achieved by inducing displacement forces from the three orthogonal slice selection and signal encoding gradient coils of a standard MRI system. The proposed method performs automatic tracking, propulsion, and computer control sequences at a sufficient rate to allow navigation along preplanned paths in the blood circulatory system. This technique expands the range of applications in MRI-based interventions. © 2007 American Institute of Physics. [DOI: 10.1063/1.2713229]

The replacement of many highly invasive procedures by minimally invasive surgeries (MIS) has been a significant milestone for modern interventional medicine.<sup>1</sup> Although the next step in modern interventional procedures<sup>2</sup> may be inspired from the 1966 science fiction movie “Fantastic Voyage,” forty years later, techniques allowing automatic navigation and directed targeting of untethered objects, devices, or microscale robots in deep regions of the human body have not been realized yet.<sup>3</sup> Medical interventional procedures relying on untethered instruments, carriers, or sensors navigating in the bloodstream could open the path to a variety of therapies, interventions, and diagnostic methods directly targeted at operative sites that remain inaccessible or at high risk to modern MIS-based instruments. In larger blood vessels, navigation of larger untethered devices may assist in applications such as reopening of encumbered arterial ways or alternative methods of aneurysm treatment, to name but a few applications. Devices released from a catheter could perform as an extension of existing MIS-based instruments.

Here, a conventional magnetic resonance imaging (MRI) system as found in many clinical settings is considered. Although MRI systems have been used exclusively for imaging purposes until now, we show that its range of potential medical and research applications can be expanded beyond imaging by this demonstrated ability of MRI scanners to provide a means of propulsion for minimally invasive devices. This

actuation method combined with imaging/tracking and control software represents the components essential for precise navigation of various types of untethered interventional devices and objects inside the human body. The use of a clinical MRI system for such applications offers many advantages including but not limited to enhanced tissue contrast, lack of radiation, and widespread availability in clinical environments. It is also shown that for navigation in larger blood vessels, the three orthogonal gradient coils inside the bore of an MRI system, typically used for slice selection and signal encoding during MR imaging, can also induce a three-dimensional (3D) directional magnetic force sufficient to propel an object made of ferromagnetic material.<sup>4</sup> This force is proportional to the amplitude of the gradient vector according to

$$\mathbf{F} = RV(\mathbf{M} \cdot \nabla)\mathbf{B}, \quad (1)$$

where  $R$  is the duty cycle of gradient generation,  $V$  the volume of the ferromagnetic object,  $\mathbf{M}$  the magnetization of the material,  $\mathbf{B}$  the magnetic field, and  $\nabla$  the vector differential operator. To navigate a spherical device in the center of larger blood vessels with Reynolds number  $1000 < Re < 3000$  and considering the retarding effect of the blood vessel walls,<sup>5,6</sup> magnetic propulsion force must overcome a drag force<sup>7</sup>

<sup>a)</sup> Author whom correspondence should be addressed; electronic mail: sylvain.martel@polymtl.ca

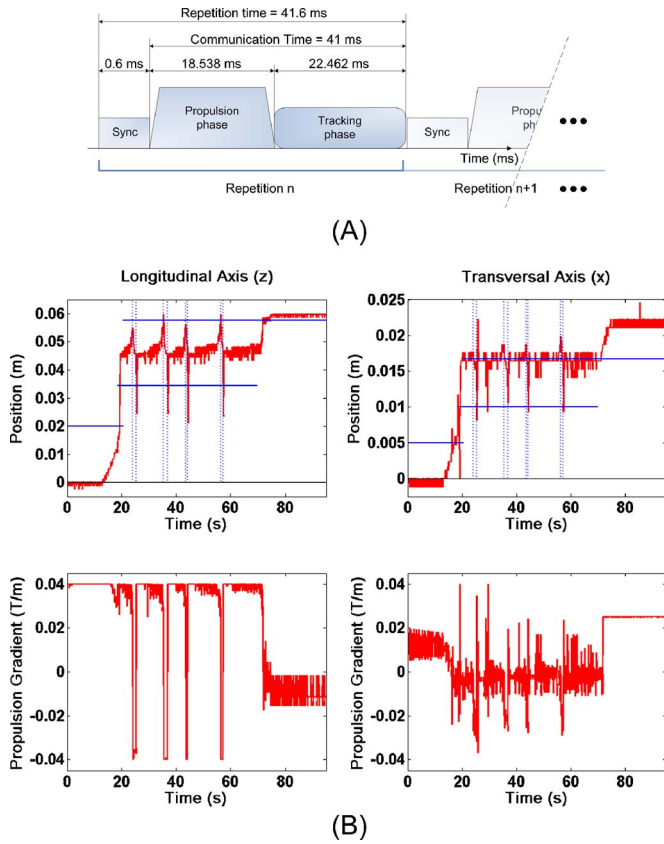


FIG. 1. (A) Overview of the real-time navigation MRI sequence for the displacement and control of the magnetic sphere. (B) *In vivo* control of a 1.5 mm ferromagnetic sphere along 11 waypoints inside the carotid artery of a living swine: tracking and propulsion gradient histories. In (a) and (c) time varying line shows sphere position along the corresponding axis. Horizontal lines represent waypoints 1, 2, and 3 targeted by the magnetic sphere. Vertical dotted lines indicate a target waypoint change during oscillation phase. (b) and (d) show gradient amplitudes as a function of time. The Y axis is not displayed for clarity since no vertical control gradients was required during this particular experiment.

$$|\mathbf{D}| = \frac{1}{2} \rho \left( \frac{u_t}{1 - \lambda^{1.5}} \right)^2 A C_{D\text{sphere}}, \quad \lambda < 0.6, \quad (2)$$

where  $\rho$  is the density of blood,  $A$  the frontal area of the immersed body,  $u_t$  the terminal velocity of the device,  $\lambda$  is the ratio between the spherical device's diameter  $d$  and the vessel's diameter, and  $C_{D\text{sphere}}$  the drag coefficient,

$$C_{D\text{sphere}} \approx \frac{24}{\text{Re}} + \frac{6}{1 + \sqrt{\text{Re}}} + 0.4, \quad 0 \leq \text{Re} = \frac{\rho u d}{\mu} \leq 2 \times 10^5, \quad (3)$$

where  $u$  and  $\mu$  are the relative velocity between the immersed device and the blood and the viscosity of blood, respectively.

Endovascular navigation made possible by integrating propulsion and tracking events within control software that deals with their time sequencing as well as with real-time, physiological, and technological constraints is presented in Fig. 1(a). The navigation sequence coordinated through custom developed proprietary software modules embedded in the MRI system consists of two events: a synchronization event responsible for the controller routine to be called that lasts for 0.6 ms and a propulsion phase and tracking acquisition event that lasts for 41 ms. While the latter event is

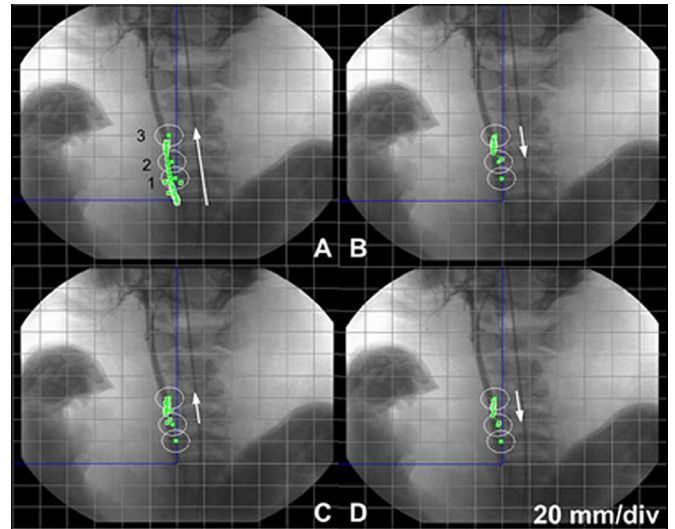


FIG. 2. *In vivo* automatic navigation of a 1.5 mm ferromagnetic bead inside the carotid artery of a living swine. The trajectories are superimposed over an x-ray angiography. The line of dots over the artery shows actual displacement of the bead. The circles (20 mm diameter) around each waypoint show precision tolerance region. Arrows show the direction of displacement. Image A, the bead travels through waypoints 1 and 2 and reaches the precision region of waypoint 3. Target waypoint changes from waypoint 2 to waypoint 3 (image B). Images C and D show two subsequent round-trips as target waypoint switches from waypoint 2 to waypoint 3 alternatively.

running, a processing time and a communication time are required for the control routine to be completed and the command to be sent to the running sequence, setting the minimum duration of the latter event with a maximum duration set by power limitations from the gradients applied during the tracking and propulsion phases. A longer duration provides more magnetic propulsion force but increases the loading level on the gradient coils and amplifiers. Hence, the 41 ms duration was determined to be the maximum level of power dissipation the MRI scanner used for the experiment could sustain.

A ferromagnetic 1.5 mm (0.0136 g) diameter chrome steel sphere (Salem Specialty Balls Company, Canton, CT) was used for the experiment. Its magnetization  $M_{1.5 \text{ T}} = 1.35 \times 10^6 \text{ A/m}$  was measured at  $B_0 = 1.5 \text{ T}$  (Walker Scientific VSM, Worcester, MA) being the field present inside the bore of the MRI system used (Siemens Magnetom Avanto 1.5 T, Erlangen, Germany). A spherical shape was chosen instead of a prolate spheroidal shape that minimizes drag force<sup>8-10</sup> since a ferromagnetic body tends to maintain its original orientation along the  $B_0$  field inside the MRI bore. Hence, the symmetry of a spherical body although not optimal for a predetermined direction of motion is still a suitable and simple compromise for general two-dimensional and 3D navigations.

The tests were performed with real-time MRI positional accuracy of 0.59 mm combined in a time multiplexed fashion with propulsion using the MRI imaging gradient coils and proportional-integral-derivative control. Real-time tracking bypassing MR susceptibility artifacts<sup>11</sup> caused by the ferromagnetic material was performed.<sup>12</sup>

A tracking data history during *in vivo* navigation of the ferromagnetic sphere being automatically controlled inside the carotid artery of a 25 kg living swine (Supplementary Movie 1, see Ref. 13) is depicted in Fig. 1(b) and Fig. 2. Ten round-trips were programmed and achieved during this test.

In Fig. 1(b), the tracking history of the sphere as well as the amplitude of the propulsion gradients in the coordinate system of the MRI platform are shown as a function of time.

In addition to the trade-off between the refresh rate and the duty cycle of the propulsion gradients [Fig. 1(a)], the time duration (repetition time) of the tracking sequence is another constraint that needs to be taken into account for optimal navigation performance. For more precise navigation subjected to perturbations, higher refresh or control rates are preferred. On the other hand, control rates beyond some thresholds can decrease tracking and propulsion performance significantly. Because of MRI signal considerations, hydrogen protons require some time duration between two subsequent rf excitations to reach an equilibrium condition. With insufficient repetition time, MRI signal acquisitions can become unusable for tracking. As a general rule, repetition time can be decreased until MR signal quality is degraded but still usable for tracking within acceptable navigational parameters such as control rate and propulsion time especially when subjected to a pulsatile flow and body movement perturbations. During the experiments, a positive  $13^\circ$  inclination of the carotid arteries with respect to the horizontal  $X$ - $Z$  plane of the MRI system was measured from a 3D MR angiography. When coupled with a potential very low friction coefficient<sup>14</sup> between the bead and the vessel, displacements of the bead when not subjected to propulsion force could occur. To reduce potential undesirable motions, a higher refresh rate of 24 Hz (41.6 ms repetition time) was chosen in this particular context to guarantee stable navigation while preserving slightly noisy but usable MRI tracking signals.

In our experimental realization of a navigable device in larger blood vessels, it is shown that automatic trajectory control of a ferromagnetic body is feasible without modifying the hardware of clinical MRI systems. Here, peak velocities in the range of 8.43–11.1 cm/s inside the artery (5 mm lumen) without blood flow have been recorded. The experimental result is less than the theoretical value of  $\sim 16$  cm/s estimated from the previous equations using  $R=44.5\%$  [Fig. 1(a)]. This difference may be caused by the presence of the balloon catheter (used to stop blood flow in the artery) sheath as well as by the eccentricity of the sphere in the vessel that is not taken into account in the wall effect correlation.<sup>5</sup>

Increasing  $\lambda=0.3$  to an optimal value (close to  $\lambda=0.42$ ) would improve performance by providing the best trade-off between propulsion force and retarding effect caused by the vessel walls.<sup>5</sup> This indicates that the design of subsequent devices would not only be guided by the types of interventional procedures but by the diameter and blood flow of the vessels used to reach the target. In turn, complex pathways involving various types of blood vessels will influence further the design of the device that could be made of a single or an agglomeration of smaller biodegradable polymeric ferromagnetic entities.

For smaller vessels, since magnetic force scales down at a cubic rate while drag force decreases linearly at low Reynolds numbers, the addition of propulsion dedicated gradient coils in the MRI bore for inducing propulsion force on a smaller device must be considered. Our preliminary data ac-

quired in this demonstration suggest that due to limits in gradient amplitudes that can be generated, the same principle but for the purpose of steering instead of propelling devices in low Reynolds hydrodynamic environments (capillaries to small arterioles or venules) could be applied. On the other hand, nanocarriers due to their single domain magnetic property behave as MRI contrast agents that already proved to be visible and traceable with MRI without causing image artefacts as it is the case for larger magnetic entities. Gradient induced magnetic forces from an MRI platform could steer agglomerations of micro- or nanodevices (or more complex devices such as nanorobots in a farther future) being drifted by blood flow. Improved targeting could be enhanced further by decreasing blood velocity with an appropriate method such as upstream balloon catheter inflation.

The results and the methods developed for this letter provide valuable data for potential future development of enhanced MIS-based interventional systems and procedures that can be adapted to a variety of applications particularly for direct delivery in nanomedicine where extensive research efforts are being made to develop multifunctional magnetic nanoparticles.<sup>15</sup>

This work was supported in part by a strategic grant from the Natural Sciences and Engineering Research Council of Canada (NSERC), in part by the Canada Research Chair (CRC) in Micro/Nanosystem Development, Fabrication, and Validation, Valorisation Recherche Québec (VRQ), and in part by the Canada Foundation for Innovation (CFI). The authors thank S. Zuehlsdorff and R. Gourdeau for discussions, G. Potvin for MRI assistance, J. Lavoie for assistance with medical instruments and procedures, and A. Lafortune for animal care.

<sup>1</sup>K. Kandarpa and J. E. Aruny, *Handbook of Interventional Radiologic Procedures*, 3rd ed. (Lippincott, Philadelphia, 2002), p. 43.

<sup>2</sup>European Medical Research Councils (EMRC) report, 2005 (unpublished). (available at <http://www.esf.org/publication/214/Nanomedicine.pdf>).

<sup>3</sup>R. A. Freitas, *J. Comput. Theor. Nanosci.* **2**, 1 (2005).

<sup>4</sup>J.-B. Mathieu, G. Beaudoin, and S. Martel, *IEEE Trans. Biomed. Eng.* **53**, 292F (2006).

<sup>5</sup>V. Fidleris and R. L. Whitmore, *Br. J. Appl. Phys.* **12**, 490 (1961).

<sup>6</sup>H. S. Munroe, *Trans. AIME* **17**, 637 (1888).

<sup>7</sup>F. M. White, *Viscous Fluid Flow*, McGraw-Hill Eeries in Mechanical Engineering, 2nd ed. (McGraw-Hill, New York, 1991), p. 182.

<sup>8</sup>O. Pironneau, *J. Fluid Mech.* **59**, 117 (1973).

<sup>9</sup>O. Pironneau, *J. Fluid Mech.* **64**, 97 (1974).

<sup>10</sup>E. Lund, H. Møller, and L. A. Jakobsen, *Struct. Multidiscip. Optim.* **25**, 383 (2003).

<sup>11</sup>S. Balac, G. Caloz, G. Cathelineau, B. Chauvel, and J. D. de Certaines, *Magn. Reson. Med.* **45**, 724 (2001).

<sup>12</sup>E. Aboussouan, O. Felfoul, J.-B. Mathieu, G. Beaudoin, and S. Martel, *Proc. Int. Soc. Magn. Reson. Med.* **14**, 3353 (2006).

<sup>13</sup>See EPAPS Document No. E-APPLAB-90-089710 for a bead being navigated inside an artery of a living swine. This document can be reached via a direct link in the online article's HTML reference section or via the EPAPS homepage (<http://www.aip.org/pub.serve/epaps.html>).

<sup>14</sup>K. Takashima, R. Shimomura, T. Kitou, H. Terada, K. Yoshinaka, and K. Ikeuchi, *Tribol. Int.* **40**, 319 (2007).

<sup>15</sup>C. C. Berry and A. S. G. Curtis, *J. Phys. D* **36**, R198 (2003).